Study of the Activation of C−H and H−H Chemical Bonds by the $[ZnOZn]^{2+}$ Oxycation: Influence of the Zeolite Framework Geometry

Luis Antonio M. M. Barbosa* and Rutger A. van Santen

Schuit Institute of Catalysis, Eindhoven University of Technology, Post Office Box 513, 5600 MB Eindhoven, The Netherlands

Received: March 31, 2003; In Final Form: September 23, 2003

The reactivity of the $[ZnOZn]^{2+}$ oxycation, located inside the zeolite micropores, has been studied by the periodical density functional method. Two different types of rings, six- and eight-membered, have been used as hosts for this cation. In addition, within each of these ring structures the arrangement of the two aluminum atoms has been explored, generating different configurations. Two different probe molecules have been used in this investigation: methane and molecular hydrogen. Both molecules prefer to chemisorb on this active site. Their dissociation reactions are strongly influenced by the surrounding zeolite environment and by the Al distribution within the zeolite ring framework. The $[ZnOZn]^{2+}$ cation is able to activate both C−H and H−H bonds, particularly the latter one. These results are in line with previous calculations and recent experimental results. They also confirm that this active site is present in high-silica zeolites. However, this species seems unlikely to be the catalytic site for the alkane dehydrogenation.

1. Introduction

Zn^{2+}-exchanged zeolites are well-known for promoting the alkane aromatization reaction.[1−12] In this process the most used zeolite is ZnHZSM-5, which has a low aluminum content. Consequently two Al atoms are unlikely to be in the same neighborhood.

During the past years, many experimental studies have focused on understanding the reaction mechanism of the dehydrogenation reaction,[1,4,7−11] as well as of the Zn-related active site in high-silica content catalysts.[8,13−17]

Some of the studies concluded that the dehydrogenation ability of the Zn cation is important in the catalytic conversion of alkanes.[1,3,7−9] The role of the Zn cation has been also proposed to enhance the recombination of hydrogen atoms and desorption of H_2, which is the rate limiting-step of the process.[7−9,11]

Among all different ideas on the possible structure of the Zn(II) active site, one interesting proposal is the formation of a $[ZnOZn]^{2+}$ cation.[3,8] This type of species has been initially suggested for other divalent cations such as Fe and Cu.[18−20]

The reactivity of this species has been evaluated earlier by theoretical calculations within different small zeolite cluster models.[21−23] The $[ZnOZn]^{2+}$ cation is rather reactive toward alkane and hydrogen dissociation, the latter being the most favorable reaction, leading to the conclusion that it can indeed be considered as a possible structure for the Zn(II) active site for dehydrogenation.

Calculations have also shown that the $[ZnOZn]^{2+}$ cation formation is energetically more favorable than the formation of Zn(II) cations, if ZnO particles are employed in the preparation of Zn^{2+} exchanged zeolites from its protonic form.[21]

However, none of these studies took into account the full complexity of the zeolite framework, which has been shown to be very important for the reactivity of the catalyst.[24−28]

The first step in this direction was to study of the stability of the $[ZnOZn]^{2+}$ cation, located inside the zeolite framework, by means of periodical calculations.[29] This active site is more stable at large rings such as eight-membered ones. Furthermore, this cation stability is strongly dependent on the relative position of the Al atoms within the zeolite ring.

The present work investigates systematically the reactivity of the $[ZnOZn]^{2+}$ cation by the periodical density functional theory approach. The physisorption and chemisorption of methane and molecular hydrogen have been studied as a function of the local environment of active site within the real zeolite structure.

2. Methods

In the work reported here, all calculations were performed with the Vienna ab initio simulation package (VASP).[30,31] This code carries out periodic density functional theory (DFT) calculations (DFT) by use of pseudopotentials and a plane wave basis set. The DFT was parametrized in the local-density approximation (LDA), with the exchange-correlation functional proposed by Perdew and Zunger[32] and corrected for nonlocality in the generalized gradient approximations (GGA) by use of Perdew−Wang 91 functional.[33]

The interaction between the core and electrons is described by the ultrasoft pseudopotentials (US-PP) introduced by Vanderbilt[34] and provided by Kresse and Hafner.[35] The plane wave cutoff used here was 400.0 eV, which better describes the oxygen atom. All calculations have been performed at the Γ point of the Brillouin zone.

Chabazite framework was chosen as a prototype of the zeolite because the unit cell contains only 12 TO_2 units, which turns the calculations less expensive. This zeolite can be also prepared with diverse Si/Al ratios and its structure is composed of eight-, six-, and four-membered rings. In the present case, the ratio Si/Al = 5.0 is maintained constant in all cases. The model

* Corresponding author: e-mail tgaklb@chem.tue.nl.

10.1021/jp030394r CCC: $25.00
Published on Web 12/02/2003

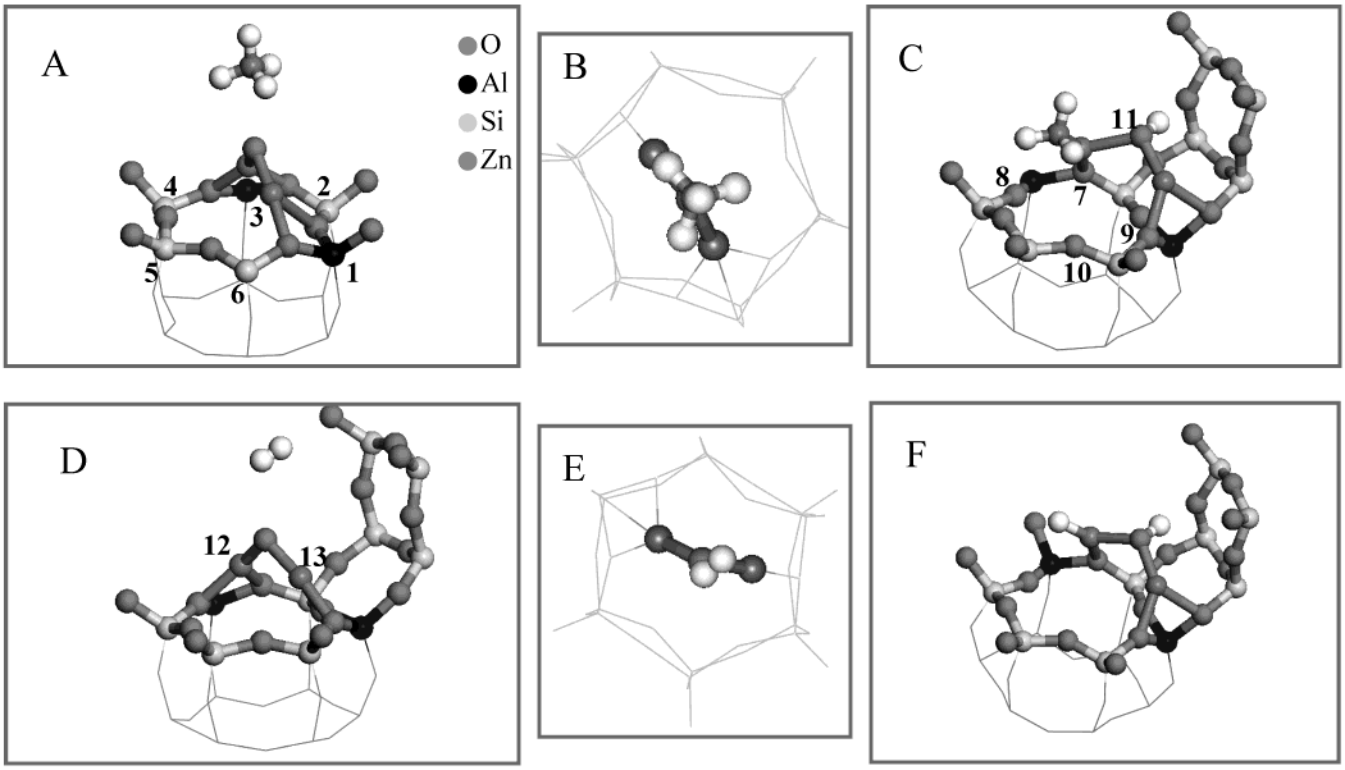

Figure 1. Six-membered ring, position 02 (AlSiAl). (A) Methane adsorption, side view. (B) Methane adsorption, top view. (C) Methane dissociative species. (D) Molecular hydrogen adsorption, side view. (E) Molecular hydrogen adsorption, top view. (F) Molecular hydrogen dissociative species.

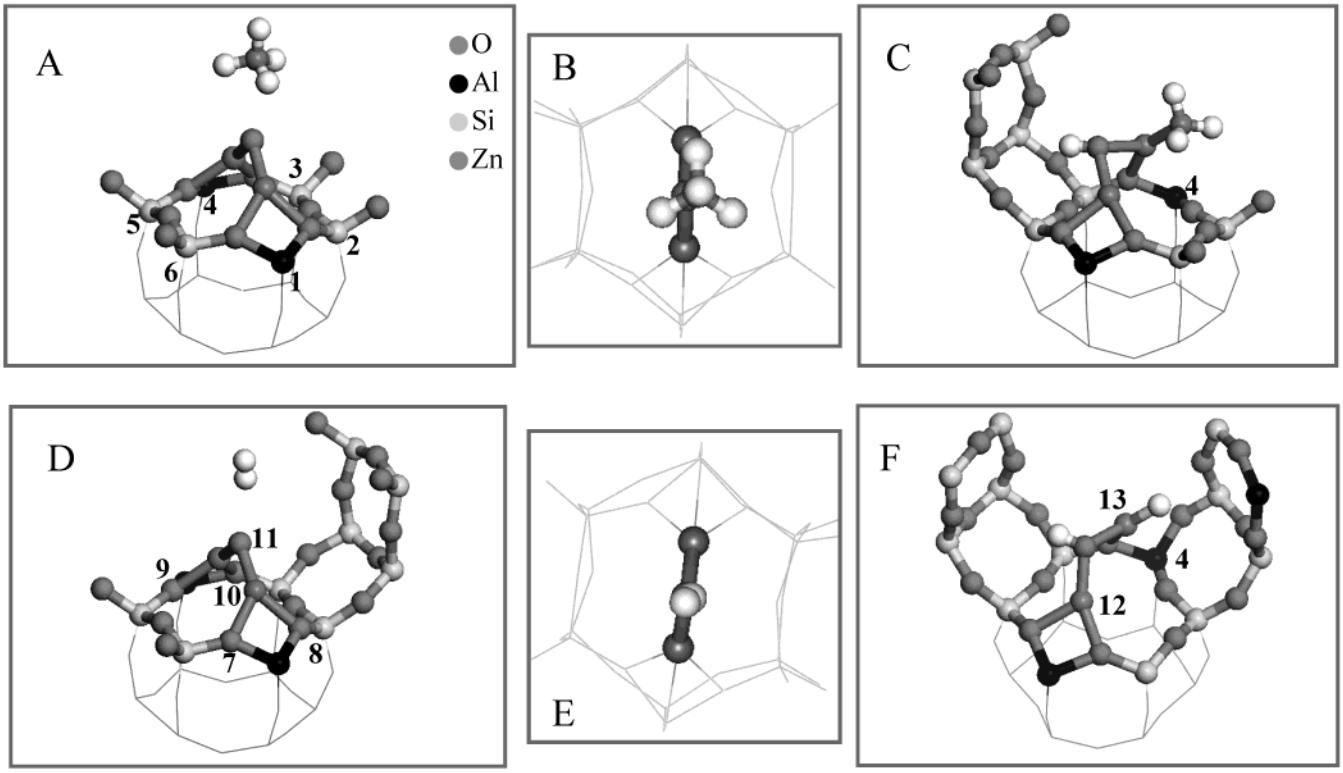

Figure 2. Six-membered ring, position 03 (AlSiSiAl). Panels A−F are as described for Figure 1.

description can be found in detail elsewhere.[24,29,36] The unit cell was optimized at a constant volume by use of a quasi-Newton algorithm. The structural parameters were considered to be converged if the forces on the atoms became smaller than 0.04 eV $Å^{-1}$.

To reduce the problems related to the residual stress, which appear due to variations of the unit cell volume, an optimization of the cell parameters has been followed. Details about this procedure can be also found elsewhere.[24,37]

The $[ZnOZn]^{2+}$ cation has been located at different ring positions: 6T and 8T, see Figures 1−6. Figure 3 corresponds to a special six-membered ring configuration, which is formed by connecting two 4T rings. In this case, each Al atom belongs to a different four-membered ring.

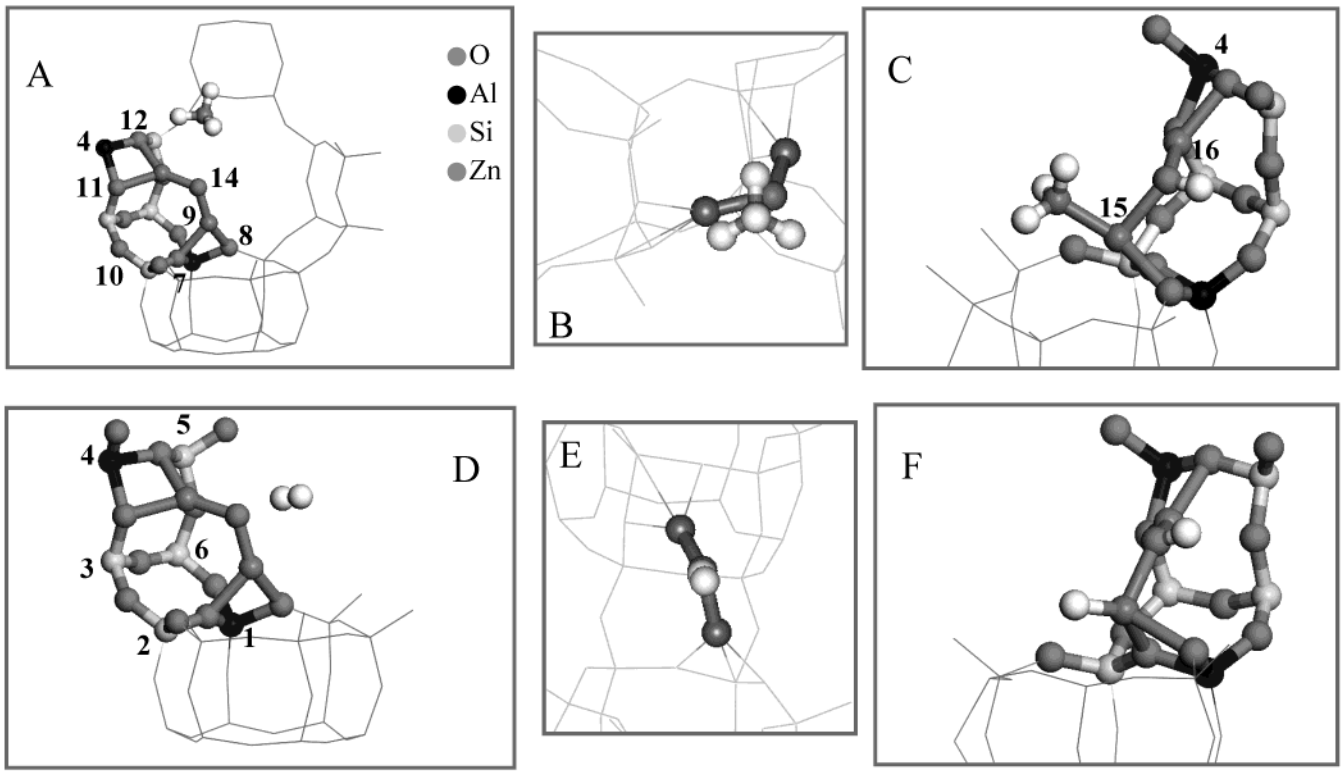

Figure 3. Six-membered ring, position 04 (AlSiSiAl). Panels A−F are as described for Figure 1.

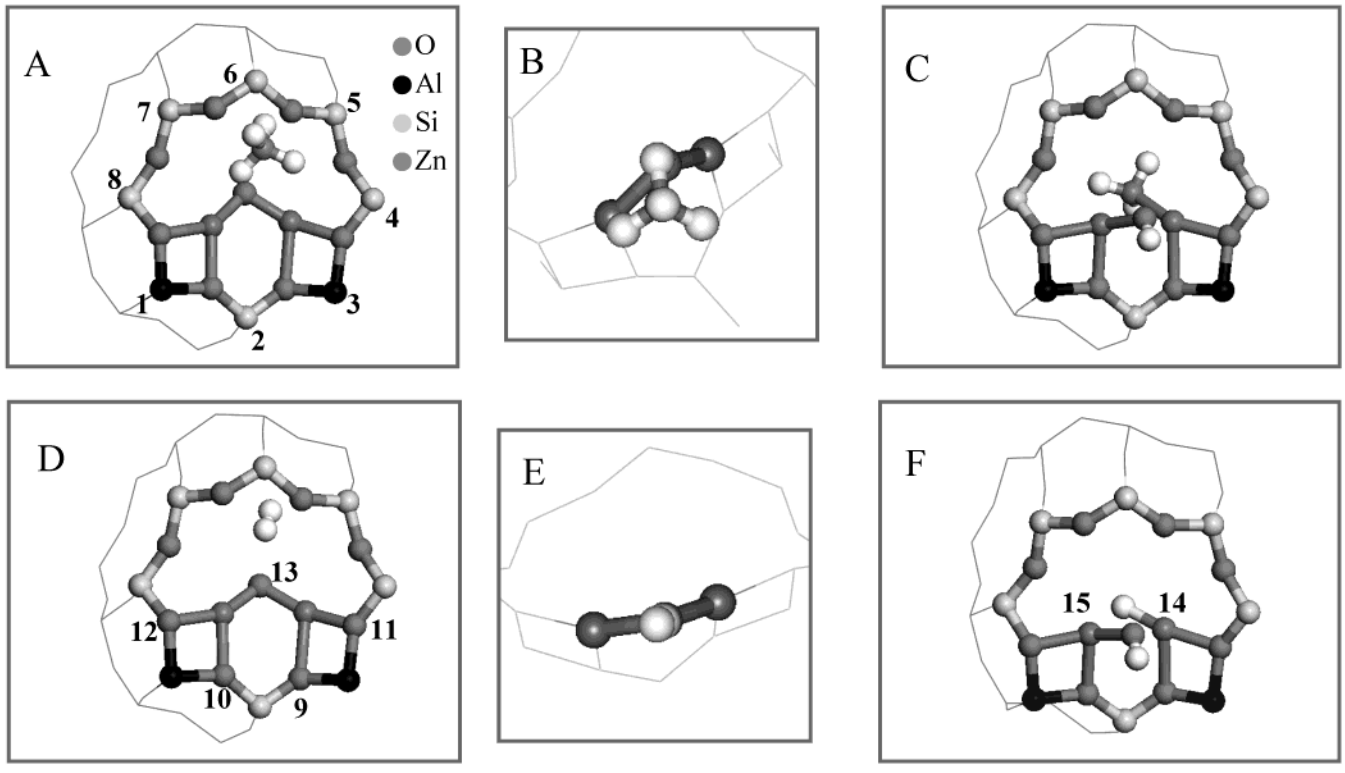

Figure 4. Eight-membered ring, position 05 (AlSiAl). Panels A−F are as described for Figure 1.

The relative positions of two Al atoms have also been explored. Therefore, each ring has more than one representation. For instance, the six-membered ring has two different possibilities for the Al atoms, positions 02 (AlSiAl) and 03 (AlSiSiAl); see Figures 1 and 2, respectively. On the other hand, the eight-membered ring has three different configurations, as seen in Figures 4−6, represented by position 05 (AlSiAl), position 05 (AlSiSiAl), and position 05 (AlSiSiSiAl).

3. Results

3.1. Molecular Adsorption on the $[ZnOZn]^{2+}$ Oxycation: Methane Adsorption. Previously, the adsorption of ethane[22] and methane[23] on the $[ZnOZn]^{2+}$ species has been explored by the cluster approach. A weak interaction between alkane and this species has been found.

The adsorption energy of methane calculated by the periodical approach is shown in Table 1. One observes that a weak

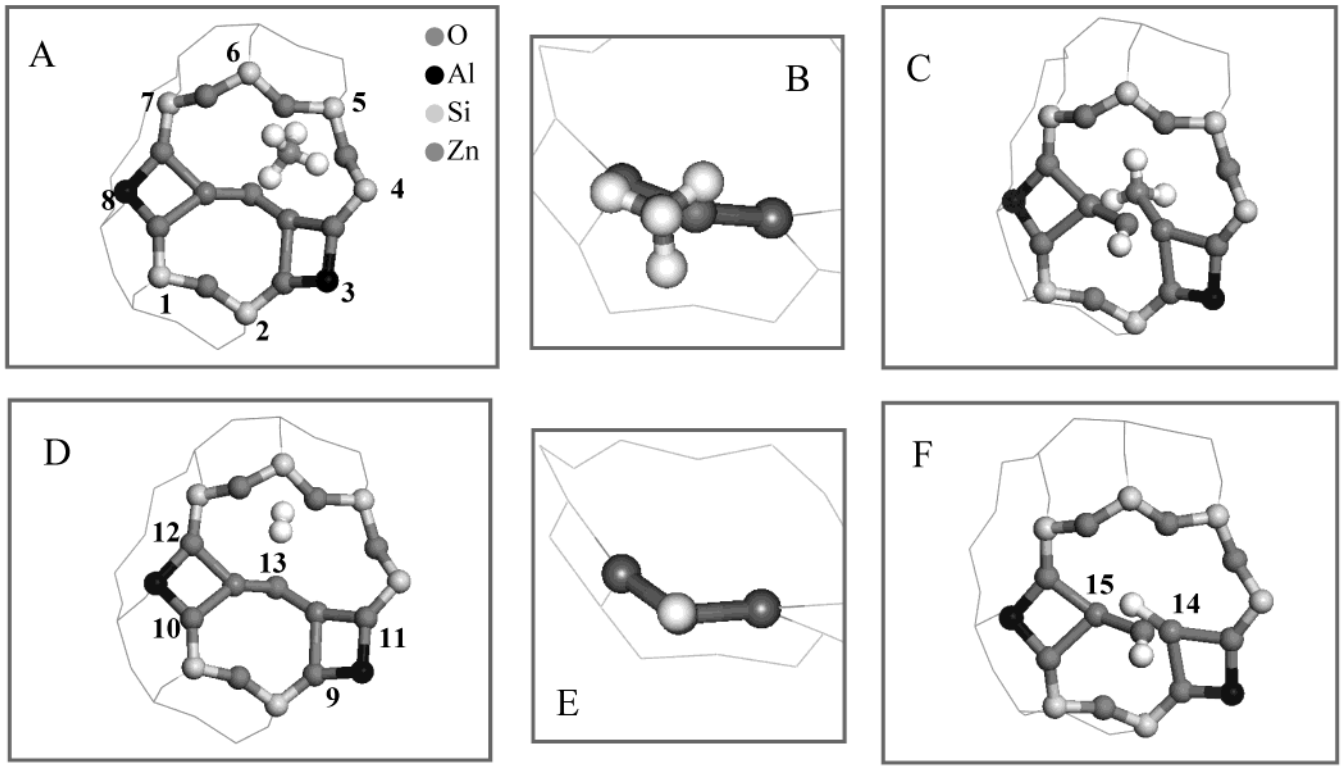

Figure 5. Eight-membered ring, position 05 (AlSiSiAl). Panels A−F are as described for Figure 1.

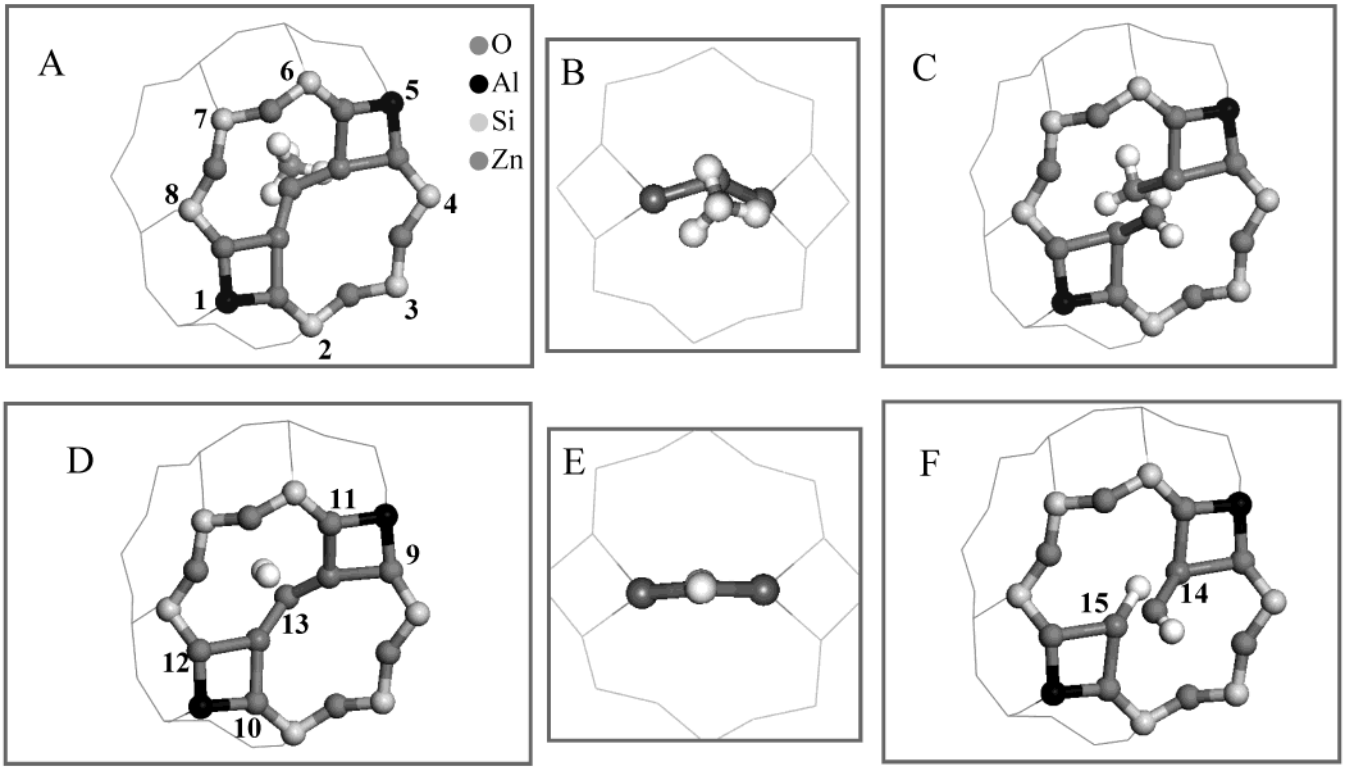

Figure 6. Eight-membered ring, position 05 (AlSiSiSiAl). Panels A−F are as described for Figure 1.

interaction is also found regardless of the position of the $[ZnOZn]^{2+}$ cation.

Upon adsorption of the probe molecule there are only slight modifications in the T−O−T angles and Zn−O distances; see Tables 2 and 3. In addition, the distance between methane and the $[ZnOZn]^{2+}$ species is almost constant and around 3.0 Å. These results agree with the idea of weak interaction between the molecule and the cation.

Methane has a C_{3v} configuration when interacting with the $[ZnOZn]^{2+}$ cation at positions 02 and 03; see Figures 1B and 2B. The same type of configuration has been described for the methane interaction with the Zn(II) cation[23,24] and ZnO cluster.[23] This C_{3v} configuration is, however, not completely attained in some positions, viz. positions 04 and 05. This change of the molecular orientation is related to the steric hindrance that methane suffers when located on these positions; see Figures

TABLE 1: Reaction Energy Values for the Different $[ZnOZn]^{2+}$ Sites[a]

	adsorption energy		dissociation energy	
type of zeolite site	methane	dihydrogen	methane	dihydrogen
Six-Membered Ring				
position 02 (AlSiAl)	−3	−8	+24	−30
position 03 (AlSiSiAl)	−4	−11	+22	−48
position 04 (AlSiSiAl)	+5	−8	−13	−79
Eight-Membered Ring				
position 05 (AlSiAl)	+7	−6	−33	−89
position 05 (AlSiSiAl)	−1	−10	−55	−118
position 05 (AlSiSiSiAl)	0	−10	−50	−110

[a] All values are given in kilojoules per mole.

3B−6B. Interestingly, such a change of the orientation has been also observed for methane adsorbed on the Zn(II) cation at position 05 (AlSiAl),[24] which confirms the influence of the zeolite framework on the adsorption mode of methane in this position.

This orientation change seems to be also correlated with the value of the adsorption energy, as seen in Table 1. However, one should keep in mind that these adsorption energies have very small values.

Hydrogen Adsorption. Molecular hydrogen is a very good probe molecule because it can interact with the active site without suffering steric hindrance. This allows the study of the interaction between this probe molecule and the $[ZnOZn]^{2+}$ species, regardless of the position inside of the zeolite framework.

One can observe in Table 1 that this molecule interacts similarly with the $[ZnOZn]^{2+}$ species at all studied positions. The molecular hydrogen is bound end-on in all cases; see Figures 1E−6E. This orientation is also preferred when molecular hydrogen is interacting with oxygen atoms of ZnO cluster.[21]

Again there are no noticeable changes in the framework structure upon hydrogen adsorption, which follows the suggestion of a weak interaction between the probe molecule and the active site; see T−O−T angles and Zn−O distance in Tables 2 and 3. The distance between molecular hydrogen and the oxygen atom of the $[ZnOZn]^{2+}$ species is also almost constant and around 2.3 Å.

The only exception for this end-on orientation is position 02, even though it is a minor change. Particularly in this position, the $[ZnOZn]^{2+}$ species is placed close to the side wall of the chabazite cage due to the relative position of Al atoms, as seen in Figure 1D,E. The molecular hydrogen interacts simultaneously with the oxygen atoms of the side wall and the $[ZnOZn]^{2+}$ species, and therefore the probe molecule cannot attain the best interaction orientation. Interestingly, the final value of the adsorption energy is similar to the other values, which indicates that there is an energy gain due to the contribution of the new interaction between the molecular hydrogen and the oxygen atoms of the framework.

It is rather difficult to associate the adsorption energy values with the stability trend found for the $[ZnOZn]^{2+}$ cation: eight-membered ring > six-membered ring.[29] However, the changes in the molecular orientation of methane upon adsorption give a good indication of how the zeolite framework influences the adsorption of probe molecules. Can the zeolite framework influence the reactivity of this active site similarly? This will be analyzed in the following part.

3.2. Dissociation on the $[ZnOZn]^{2+}$ Oxycation: Methane Dissociation. Zn-containing zeolites, especially Zn/ZSM-5, have attracted attention due to their ability to promote dehydrogenation and aromatization of light alkanes.[1−12] With the $[ZnOZn]^{2+}$ species being one of the proposed active sites for this zeolite, the dissociation of hydrocarbons on this species is one of the key points for understanding the catalytic process.

Previous theoretical studies[22,23] concluded that alkanes would follow the alkyl pathway, in which a methyl carbanion is formed during the methane activation. This is a similar

TABLE 2: Results for the Optimized Geometry for the Different Six-Membered Rings[a]

	zeolite				
	$[ZnOZn]^{2+}$	$[ZnOZn]^{2+}$-methane	$[ZnOZn]^{2+}$-H_2	$[ZnOZn]^{2+}$-CH_3	$[ZnOZn]^{2+}$-H
Position 02 (AlSiAl)					
T(1)−O−T(2)	147.3	146.9	146.3	159.6	157.4
T(2)−O−T(3)	138.3	138.8	138.0	128.7	129.3
T(3)−O−T(4)	139.6	142.0	140.7	155.1	156.1
T(4)−O−T(5)	151.0	151.0	151.4	147.6	145.2
T(5)−O−T(6)	150.3	151.0	151.2	149.7	148.5
T(6)−O−T(1)	136.2	138.1	137.7	134.7	135.7
Zn(12)−O(7)	2.04	2.04	2.05	2.02	2.02
Zn(12)−O(8)	1.99	1.97	1.97	2.84	3.01
Zn(13)−O(9)	1.88	1.88	1.89	2.00	2.00
Zn(13)−O(10)	2.73	2.63	2.58	2.66	2.51
Zn(12)−O(11)	1.81	1.80	1.81	2.14	2.04
Zn(13)−O(11)	1.76	1.77	1.77	1.84	1.85
Zn−H					1.53
O−H				0.98	0.99
Zn−C				1.95	
O−CH_4		3.02			
O−H_2			2.82		
H−H			0.75		
Position 03 (AlSiSiAl)					
T(1)−O−T(2)	139.5	139.5	139.1	129.4	136.4
T(2)−O−T(3)	161.2	156.1	156.8	158.6	145.3
T(3)−O−T(4)	136.5	140.0	139.6	147.9	147.2
T(4)−O−T(5)	139.5	142.1	140.6	132.1	130.4
T(5)−O−T(6)	149.8	150.9	151.2	146.1	151.3
T(6)−O−T(1)	141.9	141.3	141.0	151.7	148.9
Zn(12)−O(7)	2.05	2.01	2.01	2.05	2.03
Zn(12)−O(8)	1.99	2.01	2.02	1.91	1.92
Zn(13)−O(9)	2.01	2.02	2.01	2.00	2.03
Zn(13)−O(10)	2.02	2.01	2.01	2.82	2.81
Zn(12)−O(11)	1.79	1.80	1.79	1.84	1.84
Zn(13)−O(11)	1.79	1.79	1.80	2.12	2.02
Zn−H					1.52
O−H				0.98	0.98
Zn−C				1.95	
O−CH_4		3.02			
O−H_2			2.40		
H−H			0.75		
Position 04 (AlSiSiAl)					
T(1)−O−T(2)	138.9	142.2	142.0	140.0	135.4
T(2)−O−T(3)	145.2	142.8	143.2	140.9	141.0
T(3)−O−T(4)	134.5	131.6	131.8	128.6	131.9
T(4)−O−T(5)	142.0	144.4	143.9	148.7	145.4
T(5)−O−T(6)	142.0	145.8	147.0	150.0	142.2
T(6)−O−T(1)	143.5	141.5	142.0	140.6	139.5
Zn(15)−O(7)	2.14	2.09	2.10	2.25	2.14
Zn(15)−O(8)	1.96	1.97	1.97	2.12	2.18
Zn(16)−O(11)	2.00	2.06	2.03	1.95	1.95
Zn(16)−O(12)	2.23	2.11	2.10	2.09	2.16
Zn(15)−O(14)	1.79	1.79	1.79	2.09	2.04
Zn(16)−O(14)	1.80	1.80	1.79	1.83	1.84
Zn−H					1.53
O−H				0.98	0.98
Zn−C				1.96	
O−CH_4		3.17			
O−H_2			2.25		
H−H			0.76		

[a] Distances are given in angstroms, and angles are given in degrees.

TABLE 3: Results for the Optimized Geometry of the Eight-Membered Ring Positions[a]

	zeolite				
	$[ZnOZn]^{2+}$	$[ZnOZn]^{2+}$-methane	$[ZnOZn]^{2+}$-H_2	$[ZnOZn]^{2+}$-CH_3	$[ZnOZn]^{2+}$-H
Position 05 (AlSiAl)					
T(1)−O−T(2)	139.3	141.7	139.8	139.9	139.6
T(2)−O−T(3)	132.0	130.8	132.6	134.6	133.7
T(3)−O−T(4)	146.3	147.1	123.4	146.4	146.5
T(4)−O−T(5)	142.3	142.4	143.3	144.4	143.5
T(5)−O−T(6)	145.1	147.3	143.9	145.6	145.4
T(6)−O−T(7)	141.5	139.8	142.1	142.5	142.5
T(7)−O−T(8)	154.4	158.9	155.6	152.7	149.6
T(8)−O−T(1)	138.9	139.1	140.0	138.3	138.7
Zn(14)−O(9)	2.22	2.23	2.23	2.12	2.21
Zn(14)−O(11)	1.90	1.89	1.89	1.98	1.94
Zn(15)−O(10)	2.07	2.06	2.06	2.24	2.13
Zn(15)−O(12)	1.97	1.94	1.94	1.94	1.97
Zn(14)−O(13)	1.78	1.78	1.78	1.91	1.92
Zn(15)−O(13)	1.79	1.78	1.78	2.05	2.05
Zn−H					1.66/1.80
O−H				0.98	0.97
Zn−C				2.29/2.03	
O−CH_4		3.09			
O−H_2			2.25		
H−H			0.76		
Position 05 (AlSiSiAl)					
T(1)−O−T(2)	156.8	158.7	157.6	158.0	159.0
T(2)−O−T(3)	132.0	134.2	134.5	133.5	134.7
T(3)−O−T(4)	145.4	143.7	141.6	144.4	142.9
T(4)−O−T(5)	142.3	140.9	141.4	144.3	143.1
T(5)−O−T(6)	141.2	140.6	138.2	141.4	137.7
T(6)−O−T(7)	142.2	142.5	143.0	141.4	142.8
T(7)−O−T(8)	144.7	145.5	144.8	141.7	139.6
T(8)−O−T(1)	134.9	133.8	134.2	135.6	135.2
Zn(14)−O(9)	2.11	2.12	2.10	2.14	2.10
Zn(14)−O(11)	1.94	1.93	1.93	2.02	1.99
Zn(15)−O(10)	2.06	2.05	2.08	2.10	2.09
Zn(15)−O(12)	1.99	1.98	1.97	1.99	1.97
Zn(14)−O(13)	1.77	1.77	1.78	2.03	2.01
Zn(15)−O(13)	1.78	1.78	1.78	1.89	1.91
Zn−H					1.65/1.81
O−H				0.97	0.97
Zn−C				2.08/2.34	
O−CH_4		3.05			
O−H_2			2.26		
H−H			0.75		
Position 05 (AlSiSiSiAl)					
T(1)−O−T(2)	138.4	139.8	139.3	135.2	135.1
T(2)−O−T(3)	144.6	144.9	145.3	142.7	142.8
T(3)−O−T(4)	151.7	150.7	150.8	154.3	154.3
T(4)−O−T(5)	137.4	139.4	140.1	138.0	137.6
T(5)−O−T(6)	131.5	133.9	133.2	134.9	134.0
T(6)−O−T(7)	144.4	144.3	144.8	142.9	142.7
T(7)−O−T(8)	156.4	156.0	154.3	154.3	154.2
T(8)−O−T(1)	138.5	140.0	141.2	138.0	138.1
Zn(14)−O(9)	1.96	1.97	1.97	2.06	2.04
Zn(14)−O(11)	2.08	2.06	2.04	2.04	2.02
Zn(15)−O(10)	1.98	1.97	1.97	2.03	2.01
Zn(15)−O(12)	2.03	2.03	2.03	2.06	2.05
Zn(14)−O(13)	1.78	1.77	1.77	1.97	1.96
Zn(15)−O(13)	1.78	1.77	1.78	1.95	1.96
Zn−H					1.73/1.72
O−H				0.97	0.97
Zn−C				2.11/2.19	
O−CH_4		3.12			
O−H_2			2.27		
H−H			0.75		

[a] Distances are given in angstroms, and angles are given in degrees.

trend to what Frash et al.[10] have found for ethane dissociation on Zn(II) zeolites.

Here only the alkyl pathway has been considered. The configuration of the dissociative complex is shown in Figures 1C−6C, and the energy of dissociative adsorption is given in Table 1. The first point that should be observed is that methane dissociative chemisorption is exothermic for the eight-membered ring sites.

The latter result is, however, dependent on the oxycation position inside the zeolite framework. The chemisorption process becomes endothermic at both six-membered rings. These locations are surrounded by the side walls of the cage, being a rather confined position for the active site.

Upon methane dissociation, the $[ZnOZn]^{2+}$ species is transformed into two new cationic species: $[Zn(OH)]^+$ and $[Zn(CH_3)]^+$. Each of these fragments repels the other, moving toward the side wall, as seen in Figures 1C and 2C.

The first fragment ($[Zn(OH)]^+$) acquires an orientation that allows its OH group to interact with all the oxygen atoms of the side wall. This interaction favors the stability of the dissociative complex. Interestingly, the shortest OH−O(framework) distance is found for position 02 (2.12 Å) and not for position 03 (2.98 Å). This is clearly a direct consequence of the distribution of the Al atoms (AlSiAl) on the six-membered ring.

On the other hand, regardless of the Al distribution the methyl group of the other fragment suffers a steric hindrance from the side wall, thus leading to the destabilization of the dissociative complex.

The six-membered ring experiences large changes after methane dissociation, as shown by values of the T−O−T angles before and after this reaction (see Table 2). However, the six-membered ring is rather flexible,[24] which allows it to sustain distortions without large energetic penalties. Thus, the complex destabilization seems indeed to be related to the steric hindrance of the $[Zn(CH_3)]^+$ fragment.

The other six-membered ring (position 04) is placed on the lateral walls of the chabazite cage, thus leading to less steric interaction between the methyl group and the zeolite framework; see Figure 3. In addition, the two four-membered rings that form this position do not suffer large distortions; see values of the T−O−T angles (Table 2). Consequently, the dissociative process becomes exothermic.

The largest values for the dissociation energy are calculated for the eight-membered ring family. The dissociated product suffers much less steric hindrance from the side walls. In addition, there are very small changes in the T−O−T angles before and after the dissociation reaction (see Table 3), which means that distortions in the ring geometry do not directly influence the stabilization of the dissociative complex either.

Another important factor for the stabilization of the dissociative complex is the balance between the electrostatic repulsion originating from the formed cationic species ($[Zn(OH)]^+$ and $[Zn(CH_3)]^+$ and the charge stabilization of these species by the oxygen atoms of the framework.

The electronic density of the zeolite ring is shared among all oxygen atoms of the ring with a slightly larger contribution on the ones bonded to Al atoms.[28] Thus the closer the cationic species are to the oxygen atoms, the better the stabilization of the charge by electrostatic interactions. This stabilization is very well demonstrated by the high coordination number that extraframework cations have with the oxygen atoms of zeolite rings.[21,24,38]

This effect can be evaluated here by the Zn−O bond length. On average, the value of this bond is similar for all eight-membered ring cases, 2.07 Å for 05 (AlSiAl), 2.06 Å for 05 (AlSiSiAl), and 2.05 Å for 05 (AlSiSiSiAl). However, after

investigation of each of the four Zn−O distances separately, a trend appears. Individually, each Zn−O bond has a similar value when the Al atoms are largely separated within the zeolite ring, for instance, at position 05 (AlSiSiSiAl). This favors a balanced distribution of the bonds between each fragment and the oxygen atoms. On the other hand, when both Al atoms are closer, for instance at position 05 (AlSiAl), the Zn−O bonds have different values, which leads to an unbalanced distribution (see Table 2). An intermediary result occurs for the other eight-membered ring case, position 05 (AlSiSiAl).

The electrostatic repulsion between the cationic species can be evaluated by the Zn−Zn distance. The calculated values for this distance are 2.45, 2.58, and 2.55 Å for 05 (AlSiAl), 05 (AlSiSiAl), and 05 (AlSiSiSiAl), respectively. Obviously, the distinct Zn−O bond value at position 05 (AlSiAl) is a result of this repulsive interaction between the cationic fragments. Furthermore, the electrostatic repulsion is similarly reduced at the other two eight-membered ring positions, in which both Al atoms are largely separated.

Combining qualitatively both results, the final trend for the stabilization of the cationic species is the same found for the dissociation energy in the eight-membered ring family: 05 (AlSiSiSiAl) ≃ 05 (AlSiSiAl) > 05 (AlSiAl), which confirms the influence of electrostatic interactions on the stabilization system. In addition, these electrostatic effects are closely related to the Al atom distribution within the ring.

Returning to the previous case (six-membered family), the electrostatic repulsion between the cationic species should be, in combination with the $[Zn(CH_3)]^+$ steric hindrance, the cause for the destabilization of the dissociative complex at the confined positions 02 and 03.

Hydrogen Dissociation. In this case the cationic species, formed after the molecular hydrogen dissociation, are $[Zn(OH)]^+$ and $[Zn(H)]^+$.

The first point to be noted is that the dissociation reaction is favorable in all studied positions, clearly indicating that the $[Zn(H)]^+$ fragment does not suffer the same steric hindrance as $[Zn(CH_3)]^+$ in the most confined locations (the two six-membered rings).

For the six-membered family, the energy trend can be explained by the electronic stabilization of the cationic fragments. For example, the average value for Zn−O bond length at position 02, 03, and 04 is 2.38, 2.20, and 2.10 Å, respectively. This indicates that the electronic stabilization of the cationic fragments by the oxygen atoms of ring is larger at position 04 (AlSiSiAl), which is formed by two four-membered rings.

Obviously, the electrostatic repulsion between the cationic species also plays an important role in the stabilization of the cationic species. Similarly to the methane case, it is more relevant for the confined positions (02 and 03).

Although the six-membered ring is known to stabilize better the Zn(II) cation than the four-membered ring,[24] the trend found here is the opposite. This can be understood by the difficulty that both cationic species have to occupy simultaneously a closer position to the oxygen atoms of the six-membered ring. This is directly linked to the confined location of this ring in the chabazite framework; see Figures 1F and 2F. The same does not occur at position 04, in which each of these fragments is placed on a separate four-membered ring; see Figure 3F.

For the eight-membered family there is a large structural similarity between both dissociative species (methane and molecular hydrogen). For instance, the Zn−Zn distance is 2.47, 2.55, and 2.58 Å for positions 05 (AlSiAl), 05 (AlSiSiAl), and 05 (AlSiSiSiAl), respectively. In addition, the Zn−O bonds have also close values, as clearly seen from Table 3. Therefore, it is logical to conclude that both species are stabilized in the same way by the eight-membered ring and that the cationic fragments have similar electronic repulsion.

In the hydrogen dissociation case, the main factor for stabilization of the final complex is the reduction of electrostatic repulsion, associated with the better electrostatic stabilization of the cationic species by the oxygen atoms of the framework.

4. Discussion

As shown in the current study, methane and molecular hydrogen prefer to dissociatively chemisorb on $[ZnOZn]^{2+}$ species. Therefore, this active site is able to activate both C−H and H−H bonds, confirming the suggestion from previous calculations.[21−23] In addition, this work show for the first time the strong dependence of this activation ability on the $[ZnOZn]^{2+}$ oxycation location in the zeolite and on the local Al distribution.

Experimentally, molecular hydrogen dissociation is observed when this molecule is loaded in Zn-exchanged high-silica zeolite, which has been prepared by zinc oxide[15] or via reaction with zinc vapor.[39] The dissociation or adsorption is, however, inhibited upon sulfidation of the Zn/H−ZSM-5 catalyst.[40] Taking into account the results shown here for molecular hydrogen, these experimental observations could be explained by the presence of the $[ZnOZn]^{2+}$ species in Zn high-silica zeolite.

Considering this species as the active site for the dehydrogenation reaction of alkanes, two steps of the reaction path have been analyzed here.

The first step is the activation of the C−H bond. Methane prefers to chemisorb dissociatively on the $[ZnOZn]^{2+}$ species in agreement with the suggestion that Zn cations in Zn high-silica zeolite are involved in the dehydrogenation step.[1,3,7−9,11]

The other step is the formation/removal of molecular hydrogen. This corresponds to the inverse reaction of the dissociative adsorption of H_2. From the results shown here, the hydrogen removal from the $[ZnOZn]^{2+}$ site is unfavorable due to the high stability of the dissociated complex; see Table 1. However, Zn cations have been proven experimentally to be important for this reaction. The hydrogen recombination reaction has been suggested to be the rate-limiting step of the process.[4,7−9,11,41]

When the $[ZnOZn]^{2+}$ cation is considered as the active site for alkane dissociation, this site is found to promote the C−H activation but the hydrogen removal is inhibited. Among all studied configurations, only two positions could be suggested as the active site: position 05 (AlSiAl) or 04 (AlSiAl). However, the hydrogen recombination reaction is still endothermic.

Alternatively, the $[ZnOZn]^{2+}$ species could be considered as the "initiator" of the reaction, where alkanes dissociate, starting the dehydrogenation reaction. The actual active site is the new cationic site formed from the dissociation of the former species: the Zn(II) cation.

Several previous studies have calculated the reaction energy for the hydrogen removal from the Zn(II) cation in the zeolite. The reaction is endothermic (+20 kJ/mol) for the Zn cation located on a small ring (four-membered)[10,21,42] but becomes exothermic if the cation is located in a larger ring (five/six-membered ring): −50 kJ/ mol.[21,42] However, the Zn cation, associated with the five/six-membered rings, is almost inactive for catalysis.[21,24]

These results show that the hydrogen removal reaction from the Zn(II) cation is also difficult. To have a better comparison with the $[ZnOZn]^{2+}$ case, this reaction has been evaluated for the Zn^{2+} cation at position 05 (AlSiAl) by periodical calculations.

The calculated reaction energy for the recombination of hydrogen on the Zn^{2+} cation is +48 kJ/mol, which is about half that found for the same reaction on the $[ZnOZn]^{2+}$ species at the same location, position 05 (AlSiAl). This confirms that the hydrogen removal is more favorable when catalyzed on the Zn^{2+} cation site and is in agreement that this reaction is the limiting step of the dehydrogenation process.[4,7−9,11,41]

5. Conclusions

The reactivity of the $[ZnOZn]^{2+}$ cation, located inside the zeolite framework, has been studied by the periodical density functional method. Two different types of structures, six- and eight-membered rings, have been employed as hosts for this cation. Within each of these zeolite rings the arrangement of two aluminum atoms has been explored, creating different configurations.

Two probe molecules, methane and molecular hydrogen, have been employed to study the reactivity of $[ZnOZn]^{2+}$ species. These molecules dissociatively adsorb on this active site. For the first time it has been shown that this dissociation reaction is influenced by zeolite environment and the local Al distribution.

The $[ZnOZn]^{2+}$ cation is able to activate both C−H and H−H bonds, particularly the latter one. These results confirm that this active site is present in high-silica zeolites in accordance to previous theoretical and experimental results. However, this species seems unlikely to be the catalytic site for the alkane dehydrogenation, since hydrogen desorption is highly endothermic. However, this site can act as an initiator of the dehydrogenation reaction but the actual active site for this reaction is most likely to be the Zn(II) cation.

Acknowledgment. L.A.M.M.B. thanks Eindhoven University of Technology (TUE, The Netherlands) for the computational time in the supercomputer facilities at SARA.

References and Notes

(1) Mole, T.; Anderson, J. R.; Creer, G. *Appl. Catal.* **1985**, *17*, 141.
(2) Scurrel, M. S. *Appl. Catal.* **1988**, *41*, 89.
(3) Ono, Y. *Catal. Rev. Sci. Eng.* **1992**, *34*, 179.
(4) Dufresne, L. A.; le van Mao, R. *Catal. Lett.* **1994**, *25*, 371.
(5) Kumar, N.; Lindfors, L.-E. *Catal. Lett.* **1996**, *38*, 239.
(6) Viswanadhan, N.; Pradhan, A. R.; Ray, N.; Vishnoi, S. C.; Shanker, U.; Prasada Rao, T. S. R. *Appl. Catal.* **1996**, *137*, 225.
(7) Biscardi, J. A.; Iglesia, E. *Catal. Today* **1996**, *31*, 207.
(8) Biscardi, J. A.; Meitzner, G. D.; Iglesia, E. *J. Catal.* **1998**, *179*, 192.
(9) Biscardi, J. A.; Iglesia, E. *J. Catal.* **1999**, *182*, 117.
(10) Frash, M. V.; van Santen, R. A. *Phys. Chem. Chem. Phys.* **2000**, *2*, 1085.
(11) Yu, S. Y.; Biscardi, J. A.; Iglesia, E. *J. Phys. Chem. B* **2002**, *106*, 9642.
(12) Nicolaides, C. P.; Sincadu, N. P.; Scurrel, M. S. *Catal. Today* **2002**, *71*, 429.
(13) Kazansky, V. B.; Kustov, L. M.; Khodakov, A. Y. In *Zeolites: Facts, Figures, Future*; Jacobs, P. A., van Santen, R. A., Eds.; Elsevier Science Publishers: Amsterdam, 1989; p 1173.
(14) Uvarova, E. B.; Kustov, L. M.; Lishchiner, I. I.; Malova, O. V.; Kazansky, V. B. *Stud. Surf. Sci. Catal.* **1997**, *105*, 1243.
(15) Kazansky, V. B.; Borovkov, V. Y.; Serykh, A. I.; van Santen, R. A.; Stobbelaar, P. J. *Phys. Chem. Chem. Phys.* **1999**, *1*, 2881.
(16) Kazansky, V. B.; Borovkov, V. Y.; Serykh, A. I.; van Santen, R. A.; Anderson, B. G. *Catal. Lett.* **2000**, *66*, 39.
(17) Kazansky, V. B.; Borovkov, V. Y.; Serykh, A. I.; van Santen, R. A.; Anderson, B. G. *Catal. Lett.* **2001**, *74*, 55.
(18) Boudart, M.; Garten R. L.; W. N. Delgass, W. N. *J. Phys. Chem.* **1969**, *73*, 2970.
(19) Valyon, J.; Hall, K. *J. Phys. Chem.* **1993**, *97*, 7054.
(20) Chen, H.-Y.; Sachtler, W. M. H. *Catal. Today* **1998**, *42*, 125.
(21) Barbosa, L. A. M. M.; Zhidomirov, G. M.; van Santen, R. A. *Catal. Lett.* **2001**, *77*, 55.
(22) Yakovlev, A. L.; Shubin, A. A.; Zhidomirov, G. M.; van Santen, R. A. *Catal. Lett.* **2000**, *70*, 175.
(23) Barbosa, L. A. M. M.; Zhidomirov, G. M.; van Santen, R. A. *Phys. Chem. Chem. Phys.* **2000**, *2*, 3909.
(24) Barbosa, L. A. M. M.; van Santen, R. A.; Hafner, J. *J. Am. Chem. Soc.* **2001**, *123*, 4530.
(25) Haase, F.; Sauer, J. *Microporous Mesoporous Mater.* **2000**, *35*−*36*, 379.
(26) Ryder, J. A.; Charkraborty, A. K.; Bell, A. T. *J. Phys. Chem. B* **2000**, *104*, 6998.
(27) Sierka, M.; Sauer, J. *J. Phys. Chem. B* **2001**, *105*, 1603.
(28) Rozanska, X.; van Santen, R. A.; Hutschka, F.; Hafner, J. *J. Am. Chem. Soc.* **2001**, *123*, 7655.
(29) Barbosa, L. A. M. M.; van Santen, R. A. *J. Phys. Chem. B* **2003**, *107*, 4532.
(30) Kresse, G.; Furthmüller, J. *Comput. Mater. Sci.* **1996**, *6*, 15.
(31) Kresse, G.; Furthmüller, J. *Phys. Rev. B* **1996**, *54*, 169.
(32) Perdew, J.; Zunger, A. *Phys. Rev. B* **1981**, *23*, 8054.
(33) Perdew, J.; Wang, Y. *Phys. Rev. B* **1986**, *33*, 8800.
(34) Vanderbilt, D. *Phys. Rev. B* **1990**, *41*, 7892.
(35) Kresse, G.; Hafner, J. *J. Phys. Condens. Matter* **1994**, *6*, 8245.
(36) Jeanvoine, Y.; Ángyán, J. G.; Kresse, G.; Hafner, J. *J. Phys. Chem. B* **1998**, *102*, 7307.
(37) Demuth, T.; Hafner, J.; Benco, L.; Toulhoat, H. *J. Phys. Chem. B* **2000**, *104*, 4593.
(38) Bhering, D. L.; Ramírez-Solís, A.; Mota, C. J. A. *J. Phys. Chem. B* **2003**, *107*, 4342.
(39) Kazansky, V. B. *J. Catal.* **2003**, *216*, 192.
(40) Kazansky, V. B.; Serykh, A. I.; van Santen, R. A.; Anderson, B. G. *Catal. Lett.* **2001**, *74*, 55.
(41) Biscardi, J. A.; Iglesia, E. *J. Phys. Chem. B* **1998**, *102*, 9684.
(42) Shubin, A. A.; Zhidomirov, G. M.; Yakovlev, A. L.; van Santen, R. A. *J. Phys. Chem. B* **2001**, *105*, 4928.